

# A Comparative Study of Simulation Techniques with Multiple Point Statistics: The MPS Beauty Contest

John G. Manchuk, Steven J. Lyster, Clayton V. Deutsch

*Multiple point statistical algorithms are growing in number and complexity with our desire to generate models of the subsurface that reflect the true geological complexities therein. Deposition observed in such formations as the McMurray have been identified as fluvial and estuarine, among others, and the geological architecture cannot be reproduced using two point statistics. This paper identifies three MPS algorithms that rely primarily on the statistics of training images and conditioning data to construct categorical models, as opposed to MPS algorithms that rely on other image classification techniques. Algorithms are qualitatively assessed using two large three dimensional problems: fluvial and estuarine. Some quantitative analysis regarding algorithm complexity and computational demand is provided as well. Sequential indicator simulation is used as a base case for what is achievable with two point statistics. Other methods include the single normal equation, a Gibbs sampler approach, and an iterative algorithm based on random perturbations. The primary result of this work is to increase awareness of MPS algorithms, how they work, and make the algorithms available.*

## 1. Introduction

One of the challenges in building geological models using traditional two-point statistics is obtaining results that capture non-linear phenomena. For certain depositional environments, it is difficult to create a geologically realistic model based on the variogram. Higher order statistics are required to build models that have more complex features. For categorical models, multiple-point statistics (MPS) are used. MPS were initially proposed by Deutsch (1992) and Guardiano and Srivastava (1993). More than two points are used to describe geological patterns and reproduce them in categorical models.

Several MPS simulation algorithms have been developed for generating categorical models. They include simulated annealing (Deutsch, 1992); the single normal equation (SNE) approach (Guardiano and Srivastava, 1993; Strebelle, 2002); neural networks (Caers, 2001); a pattern recognition and simulation approach called FILTERSIM (Wu et al, 2008); and an algorithm called MPS-GS that uses a Gibbs sampling technique (Lyster, 2009). They all require training images, which are analogue models of the depositional environment. Training images are used to inform the MPS algorithms.

The purpose of this work is to describe and evaluate several of the MPS algorithms. One of the challenges of MPS modeling is checking the results. This is often done qualitatively, that is, how good or realistic the models look. Checking models quantitatively is difficult because it is usually not possible to assess MPS from the available data. It may only be possible to check that statistics such as the proportion of each category and large scale trends are reproduced. Quantitative checks of MPS must be done against the training image. Two measures include the multiple point histogram (Boisvert et al, 2007) and the distribution of runs (Mood, 1940). Models are evaluated in this work qualitatively. Other comparisons are done for the algorithms and include ease of setup, execution time, and memory requirements.

The contest portion of this work was setup as follows. Training images and conditioning data from two different depositional environments were provided to the authors. The target models that were sampled for generating conditioning data were withheld. Each participant generated an MPS realization using a different algorithm and provided: 1 - the executable; 2 - source code; 3 - parameter file with chosen parameters, and; 4 - the resulting model. Agreement to return all four components was required to be a participant. All algorithms were re-compiled and executed on the same computer to ensure accuracy and fairness in computational comparisons. All code and examples are provided as supplementary material.

## 2. Problem Setting and Goals

Training images and object based techniques to generate them have primarily targeted the petroleum industry. The depositional environments that are studied in this work are for reservoir modeling. Two different depositional environments are used: 1 - fluvial (Figure 1) and; 2 - estuarine (Figure 2). The fluvial deposit contains three geological objects including channels, levees, and crevasse splays that are deposited in a floodplain (Miall, 1996).

Such a deposit may be representative of North Sea reservoirs and some areas of the McMurray oil sands deposit. There are four facies to model, where each object represents a facies type. Channel, levee, and crevasse splay facies are considered net or sand facies while floodplain is non-net or shale facies.

The estuarine deposit is tide-dominated and contains channels and point bars that are embedded in cross-stratified sand. Point bars are composed of mud clast breccias and inclined heterolithic strata (IHS) that are alternating sequences of sand and shale drapes. This type of deposit architecture is characteristic of the middle McMurray formation (Ranger and Gingras, 2003). There are five facies to model: channel fill CHF, breccia BR, point bar sand PBS, shale SH, and cross-stratified sand CSS. Both the fluvial and estuarine training images are 256 by 256 by 128 pixels covering a square area of 4,096 m and a thickness of 20.48 meters. Each grid cell is 16 by 16 by 0.16 m in size.

The overall goal of this work is to describe MPS and evaluate its abilities as a tool for practitioners. Goals encompassed by this are: to briefly describe the various algorithms that are available; provide resources for each including relevant references, source code and executable programs; and to demonstrate each algorithm and provide a qualitative evaluation of their performance. For the demonstrations, all parameters and results are provided.

### 3. Sample Data

Two realizations of each type of depositional environment are generated with identical parameters. One realization is used for extracting a set of conditioning data while the other is used as a training image. Sampling is done using vertical wells on an 8 by 8 quasi-regular grid to simulate exploration or delineation sampling (Figure 3). To remove the effects of sampling for comparison of final results the target global proportions of each facies is provided (Table 1). Each data set consists of 8,192 facies samples. A cross section through each data set is shown in Figure 4 that coincides with AA' from Figure 3.

**Table 1: Target global proportions of each facies.**

Environment	Facies Name	Facies Code	Proportion	Sill
Fluvial	Floodplain	0	0.43	0.245
	Channel	1	0.44	0.246
	Levee	3	0.10	0.090
	Crevasse Splay	4	0.03	0.029
Estuarine	Cross Stratified Sand	0	0.20	0.160
	Shale	1	0.05	0.048
	Point Bar Sand	2	0.48	0.250
	Breccia	3	0.05	0.048
	Channel	4	0.22	0.172

### 4. Base Case

Sequential indicator simulation (SIS) (Deutsch and Journel, 1998) is used to provide a base case for comparison and for a qualitative evaluation example. The BLOCKSIS program developed by Deutsch (2006) is used with variograms that are derived from the training image instead of from the sparse conditioning data. Variograms are modeled in the  $x$ ,  $y$ , and  $z$  directions (Figure 5). The assumption of second order stationarity is not appropriate; however, we cannot derive local variograms from the training image and apply them to the data. All of the details in the training image cannot be summarized by the variograms and this motivates the use of MPS.

A qualitative evaluation of a realization is done by visualizing plan and cross sections of the model with those from the training image (Figure 6). This is a subjective approach because everyone observes images differently; however, we can agree that little to no features of the training image are observed in the SIS realization. Connectivity of channel and levee facies is poor. Some qualities are preserved. For example, the crevasse splay facies are thin in cross section and more symmetric and extensive aerially, as in the training image. The apparent channel thickness with some amalgamation of channels is similar in cross section because this information was entrained in the vertical variogram. The same conclusion for the thickness of other facies can be drawn. The global proportions are reproduced as is the nature of SIS. Two advantages of this approach are the

execution time and memory requirements are both low. A single realization took 4.2 minutes and utilized 301 MB of RAM.

## 5. MPS Algorithms

Algorithms described in this section include the single normal equation (SNE) approach, the Gibbs sampler approach (MPS-GS) developed by Lyster (2009), and the iterative approach developed by Deutsch (updated in this CCG report). The SNE approach is the most intuitive approach for modeling with MPS. When applied in a naive fashion, it is also the most straightforward to apply; however, implementing it in a computationally efficient way is more challenging than the other methods.

### SNESIM

The SNE approach implements Bayes' Law, Equation (1), which defines the probability of an event,  $A$ , occurring based on a pattern of other events,  $B$ , that have already occurred.

$$P(A|B) = \frac{P(A \cup B)}{P(B)} \quad (1)$$

In the context of categorical geological modeling,  $A$  is the probability that a particular category exists at an unsampled location and  $B$  is a pattern of sampled categories near  $A$ .  $P(B)$  is the probability that defines how common the pattern is in the domain of interest (Figure 7). Computing the probability that each category exists at  $A$  is done using training images. A training image is scanned for all occurrences of the pattern  $B$  and for each one, the category at  $A$  is recorded. The number of times each category occurs at  $A$  divided by the number of times the pattern  $B$  is found in the training image is the probability of interest. Refer to Strebelle (2000) for more detail. Incorporating these probabilities into a categorical modeling algorithm is described in the following for each location,  $\mathbf{u}$ , in a domain of interest:

1. Search for nearby data that may be existing samples or previously simulated data at other locations. The data found forms a pattern,  $B$ .
2. Scan the training image for  $B$  and compute the probability that each category exists at  $\mathbf{u}$ .
3. Convert the probabilities into a cumulative distribution function (CDF).
4. Draw a category from the CDF and add it to the pool of previously simulated categories.

In the naive implementation, the training image is scanned for every different pattern  $B$  encountered. More computationally efficient implementations involve discrete templates (Figure 7) that restrict the size of patterns as well as search trees that store a compressed version of all the patterns that exist in a training image. Instead of scanning the training image repeatedly, probabilities are extracted from the search tree (Strebelle, 2000 and 2002). Patterns may also be compressed using neural networks (Caers, 2001). It is possible to introduce more advanced features in the SNE algorithms such as the ability to reproduce global proportions and local proportions from trend models and improved feature reproduction using multiple grids.

### MPS-GS

The Gibbs sampler MPS simulation method is an iterative technique that uses multiple-point events to determine the conditional probability of a facies at a given location (Lyster and Deutsch, 2008; Lyster, 2009). A multiple-point event is a discrete set of  $N$  points distributed spatially within a template. Limiting the size of each event (for example,  $N = 4$ ) allows a larger MPS template to be used without increasing the order of the statistics,  $K^N$ , where  $K$  is the number of categories, to too high a value for inference from a training image. The template must be segmented into  $M$  sub-templates, each having  $N$  points (Figure 8) and probabilities from each sub-template are combined using the normal equations as described by Lyster (2009).

Training images are used to calculate the probability that each facies occurs at the central position in the template based on the multi-point histogram observed in each of the sub-templates. These are described as multi-point events (MPE). Based on the segmented template in Figure 8 and assuming there are four categories, the total number of probabilities is  $MK^N = 7 \cdot 256 = 1,792$ .

After scanning a training image and storing all probabilities, the following workflow is used by the MPS-GS algorithm:

1. Generate an initial categorical realization.
2. For each location,  $\mathbf{u}$ , in the model:
  - i. Estimate the conditional probabilities of each category based on the MPE's from the training image and initial realization.
  - ii. Convert the probabilities into a CDF.
  - iii. Draw a category from the CDF and update the initial realization.
3. Check for convergence of the MPE statistics from the realization to the training image. Repeat step 2 until convergence is reached.

Unlike the SNE approach where a realization is generated on a grid from conditioning data, or no data in the unconditional case, the MPS-GS algorithm requires an initial realization that is updated with an iterative approach. The initial realization may be generated randomly; however, much better convergence rates are obtained if the initial image contains some of the desired features. Methods such as SISIM or the SNE approach could be used to accomplish this. Additional features to reproduce global proportions and local proportions from trends as well as user-defined templates and multiple gridding are possible with the MPS-GS algorithm as well.

#### **Simulated Annealing (different algorithm now)**

An iterative approach is adopted. A random category from the local proportions is assigned at each location. The conditioning data are fixed and never permitted to change. The grid nodes are all visited in a random order spiraling away from the conditioning data to ensure that they are reproduced without a discontinuity. Normally, 5 to 15 loops through all grid nodes will ensure convergence of the final realization. When a grid node is visited a number of steps are taken: (1) an alternative category is considered, (2) all objective functions are updated and combined into a change in the global objective function, (3) a change may be made to the current category if the objective function improves. These random perturbations are remarkably effective at permitting convergence of an initially random realization toward one that satisfies all of the constraints.

### **7. Results and Evaluation**

The three algorithms described in the previous section were used to generate a categorical realization for the fluvial case and for the estuarine case. Tuning parameters used for each algorithm and case are described and qualitative discussions of the results are given. Algorithms are also compared for ease of use, execution time, and computer memory demand. A script that generates several plan views and cross sections whose location is chosen based on the target models is applied to all entries. How well features from the training image are reproduced in the resulting views is checked. Comments will be objective so that readers can draw their own conclusions. For the fluvial model, plan views were chosen at  $z$  cell indexes 4, 44, and 112; cross sections in the  $xz$  plane were chosen at  $y$  cell indexes 44, 128, and 213; cross sections in the  $yz$  plane were chosen at  $x$  cell indexes 44, 128, and 213 as well. An example of the output is shown in Figure 6. For the estuarine model, plan views were chosen at  $z$  cell indexes 24, 63 and 100. Cross sections are the same as for the fluvial model.

A summary of the quantitative results is provided in Table 2. Tuning parameters include any that are used to change the appearance of results, such as the variogram, search ellipsoid, number of conditioning and previously simulated values to use, servosystem factors, and others. It is used to give a concept of algorithm complexity from the user's point of view. Even though parameters such as the variogram consist of several components, they are counted as a single tuning parameter. For reference, an algorithm having 10 parameters would be considered complex, but very flexible; whereas an algorithm with no parameters is basic, but inflexible.

**Table 2: Overview of algorithm performance.**

Algorithm Used	Number of Tuning Parameters	Memory Requirements (GB)	Time/Realization + Overhead (min)
BLOCKSIS	4	0.30	4.2
SNESIM	2	6.62	8.5
MPS-GS	7	1.46	5.5 + 152.9

## SNESIM

A version of SNESIM from Strebelle (2000) was used and a complete description of parameters can be found therein. Parameters used for the fluvial and estuarine cases were as follows: servosystem parameter  $\mu = 0.5$ , search radii of 800 m in  $x$  and  $y$  and 5 m in  $z$  for the fluvial case, search radii of 500 m in  $x$  and  $y$  and 5 m in  $z$  for the estuarine case. Parameters such as the search template, number of conditioning and previously simulated data to use, and number of multigrids are determined automatically by the algorithm. Results for the fluvial case are shown in Figure 9. Plan views are similar to the training image; however, there is more short range variability in the result and less connectivity of channel and levee facies. Cross sections are very similar to the training image and show good reproduction of object geometry and organization. Levees are generally adjacent to channels and crevasse splays form small aerielly-isotropic clusters.

Results for the estuarine case are shown in Figure 10. Channels are quite disconnected, which is likely due to their size relative to surrounding point bar objects that tend to take precedence. Breccia objects are similar to those in the training image as are the overall appearance of the cross sections. Separate channel successions are apparent. Shale drapes are reproduced well despite their low proportion and small size; however, their arc shape in plan view was not retained.

The version of SNESIM used was straightforward to implement, with complex parameters chosen automatically by the algorithm; however, for expert use this does impose some limitation and one may find it difficult to obtain desirable results. In this case, other expert versions are available. Setting up the parameters and executing the algorithm to obtain results was relatively painless. Some fine tuning of the search parameters was necessary to arrive at the best looking realization. The algorithm is memory intensive, requiring 6.62 GB for these cases. It took approximately 8.5 minutes to generate a realization.

## MPS-GS

For a complete description of MPS-GS parameters, see Lyster (2009). Parameters used for the fluvial and estuarine cases were as follows: five multi-grids;  $M = 12$  sub-templates or MPE's;  $N = 4$  points per sub-template; servosystem parameter  $\mu = 1$ ; connectivity correction factor  $\eta = 0.2$ . For the fluvial case, the minimum multiple-point frequency to consider from the training image was  $10^{-5}$  while for the estuarine case was  $5 \times 10^{-4}$ . Results for the fluvial case are shown in Figure 11. The overall architecture of the geological objects appears to be reproduced with good connectivity of channel and levee facies and smaller isotropic crevasse splays. Thicknesses of these objects look similar to those in the training image. The sectional views do not clearly show individual channels; however, some are visible in  $YZ$  section 213 with nice shaped levees at the channel fringes. Facies associations appear correct, such as levees primarily occurring adjacent to channels. There are some areas with artifacts near the conditioning data. Cross sections indicate some strings of conditioning data that appear as noise; this is caused by objects of other facies forming near the data. The top center of  $XZ$  layer 43 is a good example of this, where a high proportion of floodplain facies has encroached on an interval of levee facies in the data.

Results for the estuarine model were less successful (Figure 12). The extensive point bar sand facies is reproduced in the realization; however, the channel objects are not reproduced aerielly and the narrow channel cross sections are observed only occasionally. The shale facies does not have the draped effect that is present in the training image. Although the breccia facies appear to form laterally extensive layers, their thickness is too extensive. Individual geological successions are not reproduced clearly. Global facies proportions were approximately reproduced, but as in the fluvial case the lower-frequency facies, shale and breccia, had a relatively higher mismatch proportional to their target frequencies. There are some artifacts near conditioning data similar to the fluvial case. Overall, the complexity of the geology makes this type of estuarine environment a poor candidate for modeling with MPS-GS.

For ease of use, MPS-GS requires expert input judgement as there are many parameters to tune including number of multigrids to use, number of multi-point events to consider, points per event, minimum multi-point frequency, template design, stopping criteria, a servosystem parameter, and a connectivity correction factor (Lyster, 2009). Memory requirements were 1.46 GB and execution time was 158.4 minutes: 152.9 to compute the multi-point statistics and 5.5 minutes for the realization. Generating additional realizations does not require re-computing the multi-point statistics. An advantage of the MPS-GS approach is that an initial image can be specified. For example, SNESIM could be used to generate an initial image, then MPS-GS could be used to adjust it and hopefully enhance the results.

### **Iterative Algorithm**

The parameters for this algorithm were quite straightforward and only one program is required. Small models are constructed very quickly, but large models take significant CPU time. The time required for the large 3-D model of this contest was about eight hours – too long for effective comparison. Some refinements are being considered.

### **8. Conclusions**

This paper has drawn attention to some of the MPS simulation algorithms that could be used for modern geostatistical simulation. This will be updated with new algorithms and will provide the practitioner with a place to find relevant programs and test cases.

### **References**

- Boisvert, J.B., Pyrcz, M.J., Deutsch, C.V. (2007) Multiple-point statistics for training image selection. *Natural Resources Research*, 16(4), 313-321
- Caers, J. (2001) Geostatistical reservoir modeling using statistical pattern recognition. *Journal of Petroleum Science and Engineering*, 29(3): 177-188
- Deutsch, C.V. (1992) Annealing techniques applied to reservoir modeling and the integration of geological and engineering (well test) data. PhD Thesis, Stanford University, Stanford, CA. 306 pages
- Deutsch, C.V. and Journel, A.G., (1998) GSLIB: geostatistical software library and user's guide. Oxford University Press, 384pp.
- Deutsch, C.V. (2006) A sequential indicator simulation program for categorical variables with point and block data: BlockSIS. *Computers & Geosciences*, 32, 1669-1681
- Guardiano, F. and Srivastava, M. (1993), Multivariate geostatistics, beyond bivariate moments. In Soares, A. (ed), *Geostatistics Troia '92*. Vol. 1, 133-144
- Lyster, S.J. and Deutsch, C.V., (2008) MPS simulation in a Gibbs sampler algorithm. *Proceedings 8<sup>th</sup> International Geostatistics Congress, Santiago, Chile*, 1, 79-86
- Lyster, S.J. (2009) Simulation of geologic phenomena using multiple-point statistics in a Gibbs sampler algorithm. PhD Thesis, University of Alberta, Canada, 246 pages
- Miall, A.D. (1996) *The geology of fluvial deposits: sedimentary facies, basin analysis and petroleum geology*. Springer-Verlag, Berlin, 582pp.
- Mood, A.M. (1940) The distribution theory of runs. *Annals of Mathematical Statistics*, 11(4), 367-392
- Ranger, M.J., Gingras, M.K. (2003) *Geology of the athabasca oil sands: field guide and overview*. Canadian Society of Petroleum Geologists, Calgary, 123pp.
- Strebelle, S. (2000) Sequential simulation drawing structures from training images. PhD Thesis, Stanford University, Stanford, CA. 187 pages
- Wu, J., Boucher, A., Zhang, T. (2008), A SGeMS code for pattern simulation of continuous and categorical variables: FILTERSIM. *Computers & Geosciences*, 34, 1863-1876

Figures

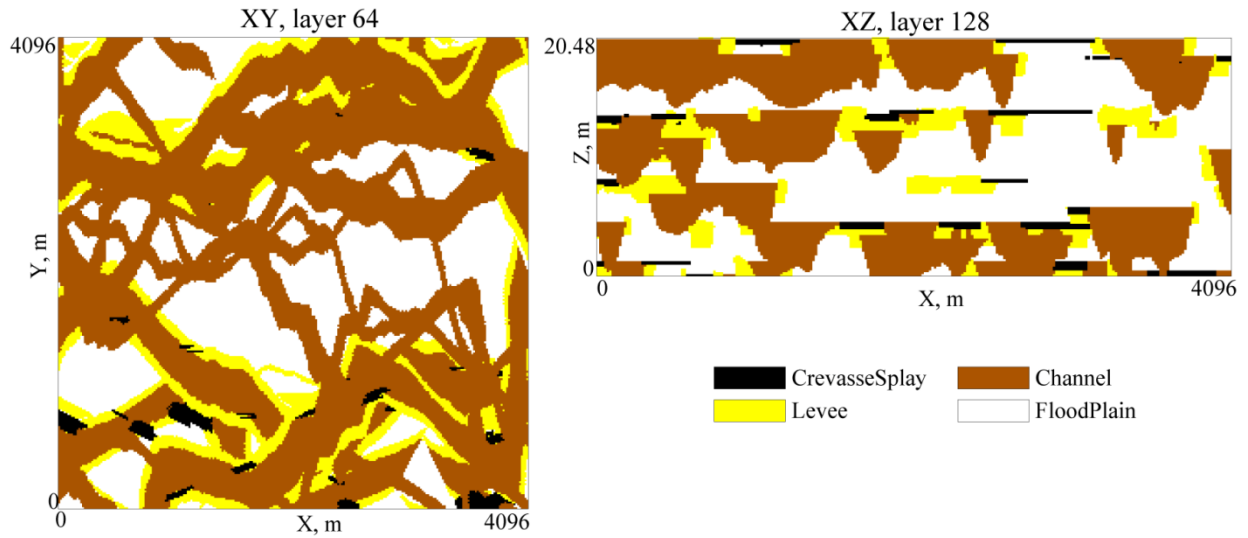


Figure 1: Plan and cross section of fluvial deposition, which is also used as the training image. A vertical exaggeration of 75 is used for the cross section.

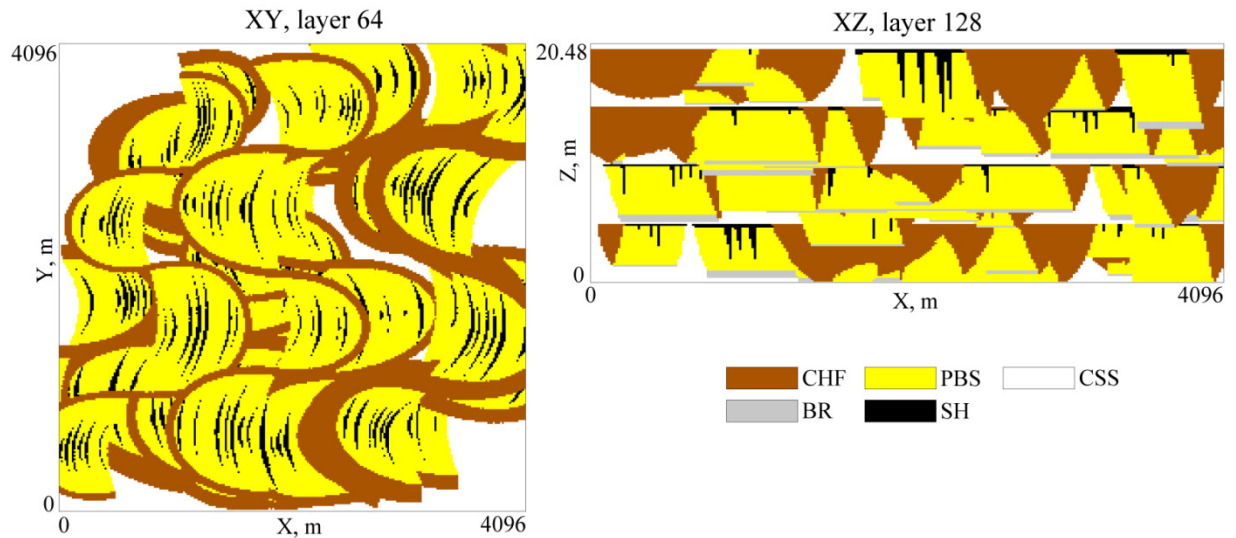


Figure 2: Plan and cross section of estuarine deposition, which is also used as the training image. A vertical exaggeration of 75 is used for the cross section.

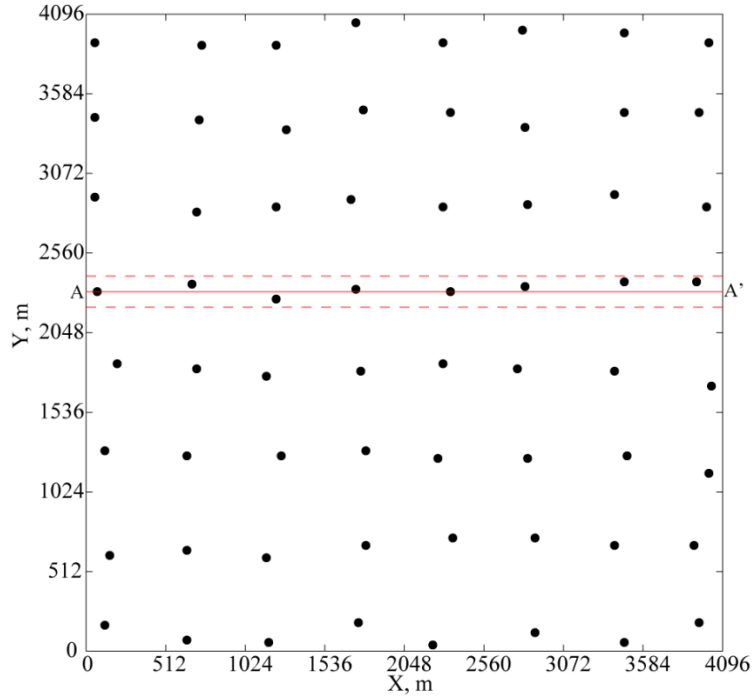


Figure 3: Sample locations and location of cross sections in Figure 4.

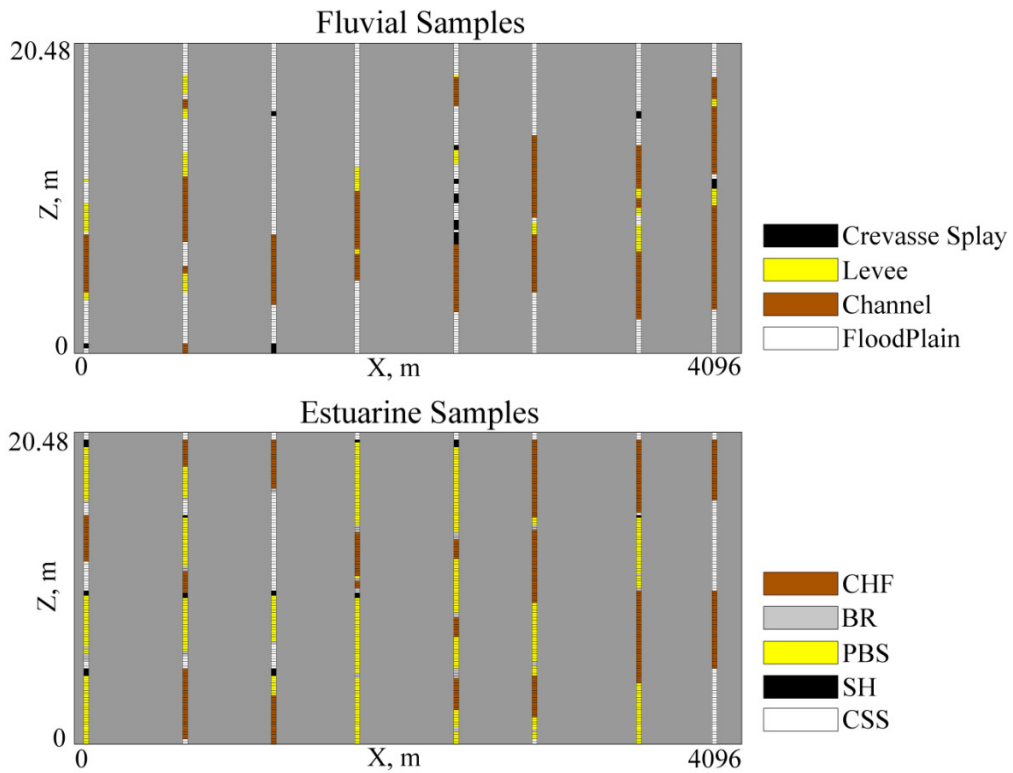


Figure 4: Cross section through  $Y = 2312 \text{ m}$  showing sample data for fluvial and estuarine environments.



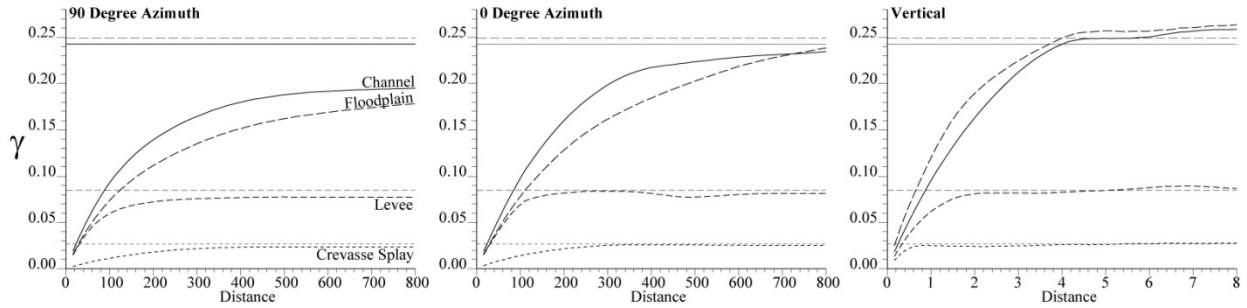


Figure 5: Experimental variograms from the fluvial training image.

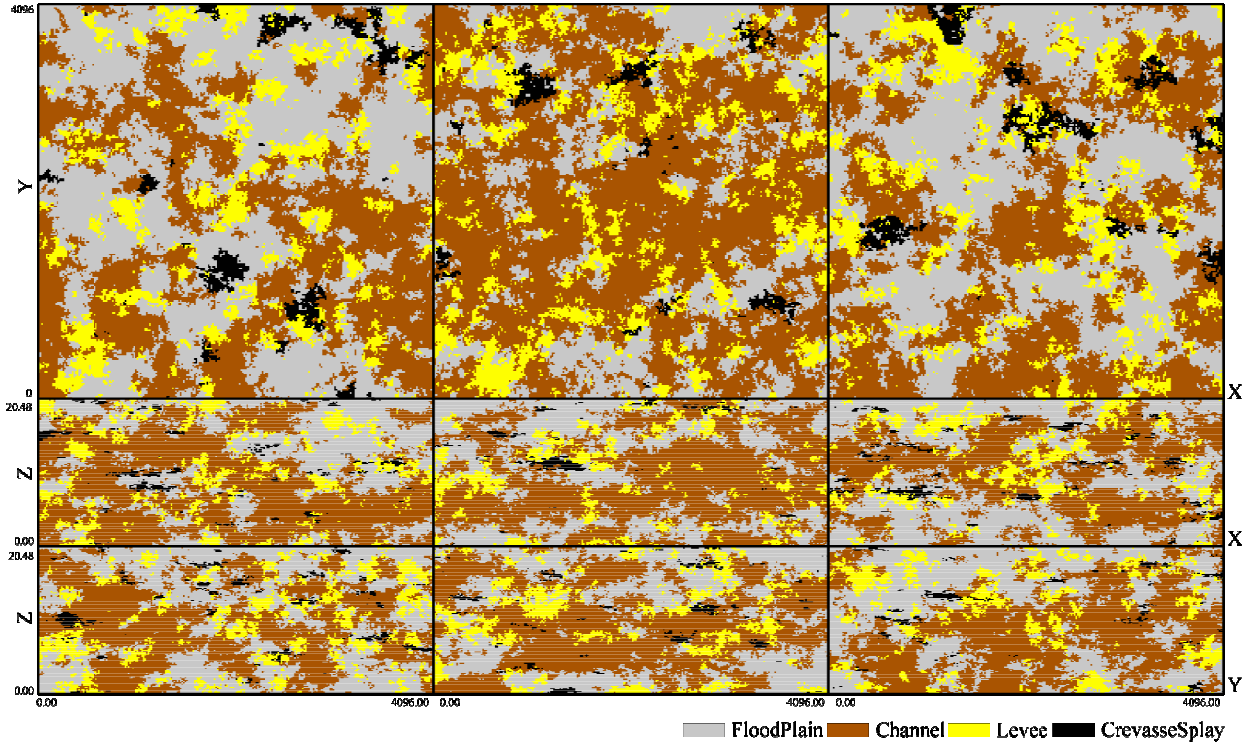


Figure 6: Plan and cross sections from a fluvial SIS realization. From upper-left to lower-right: slice 4, 44, 112; XZ sections 43, 128, 213; YZ sections 43, 128, 243.

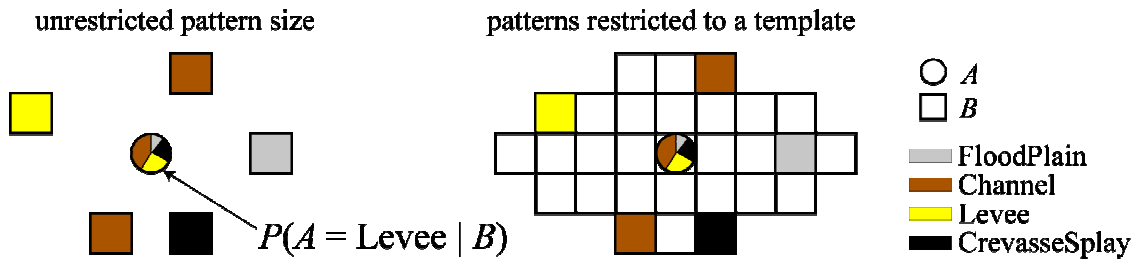


Figure 7: Example pattern  $B$  and probabilities for  $A$  using facies from the fluvial setting. The same pattern is also shown in a template of grid cells commonly used to limit the pattern sizes explored in a training image.

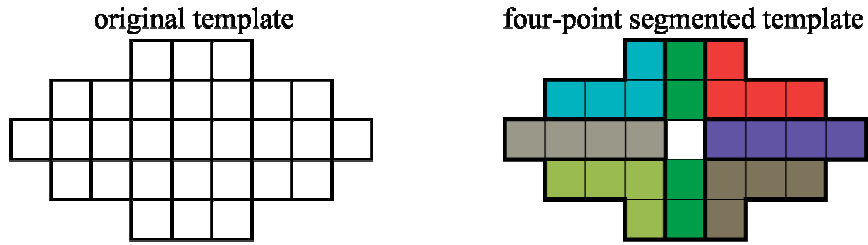


Figure 8: A pattern template segmented into  $M = 7$  sub-templates, each with  $N = 4$ . There is no limitation on how the template is segmented.

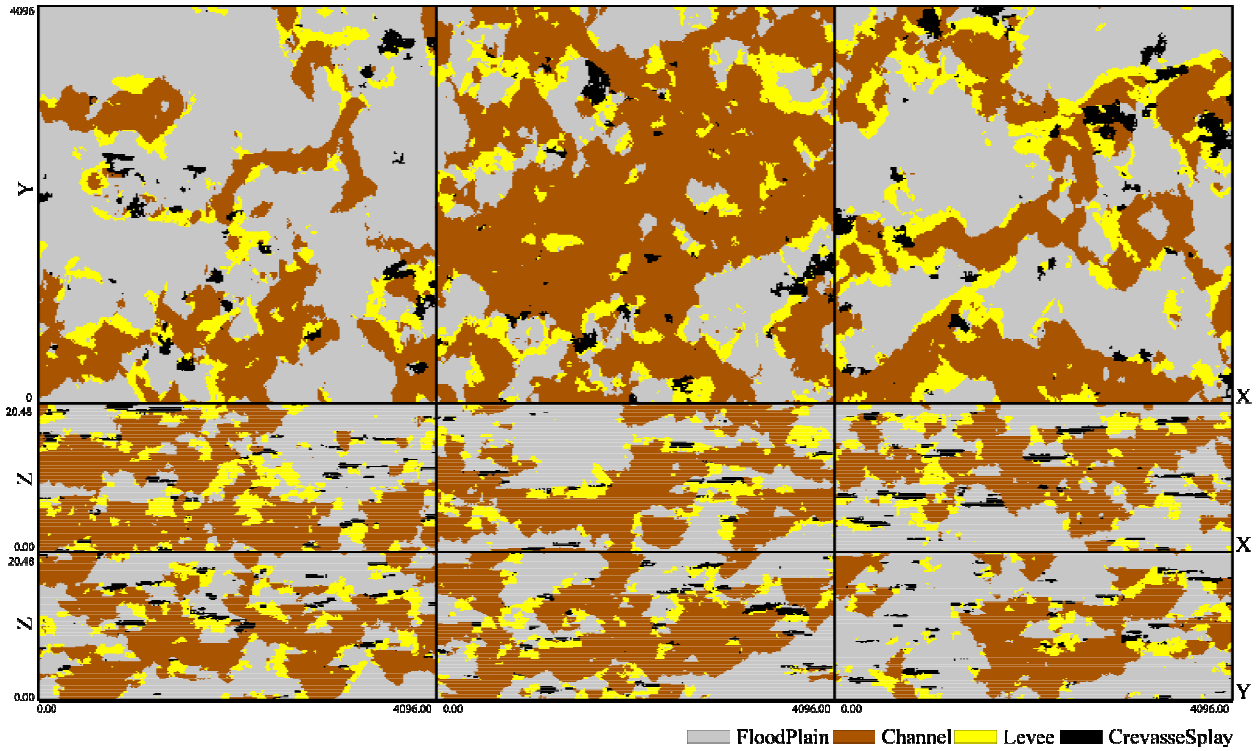


Figure 9: Fluvial SNESIM realization. From upper-left to lower-right: slice 4, 44, 112; XZ sections 43, 128, 213; YZ sections 43, 128, 243.

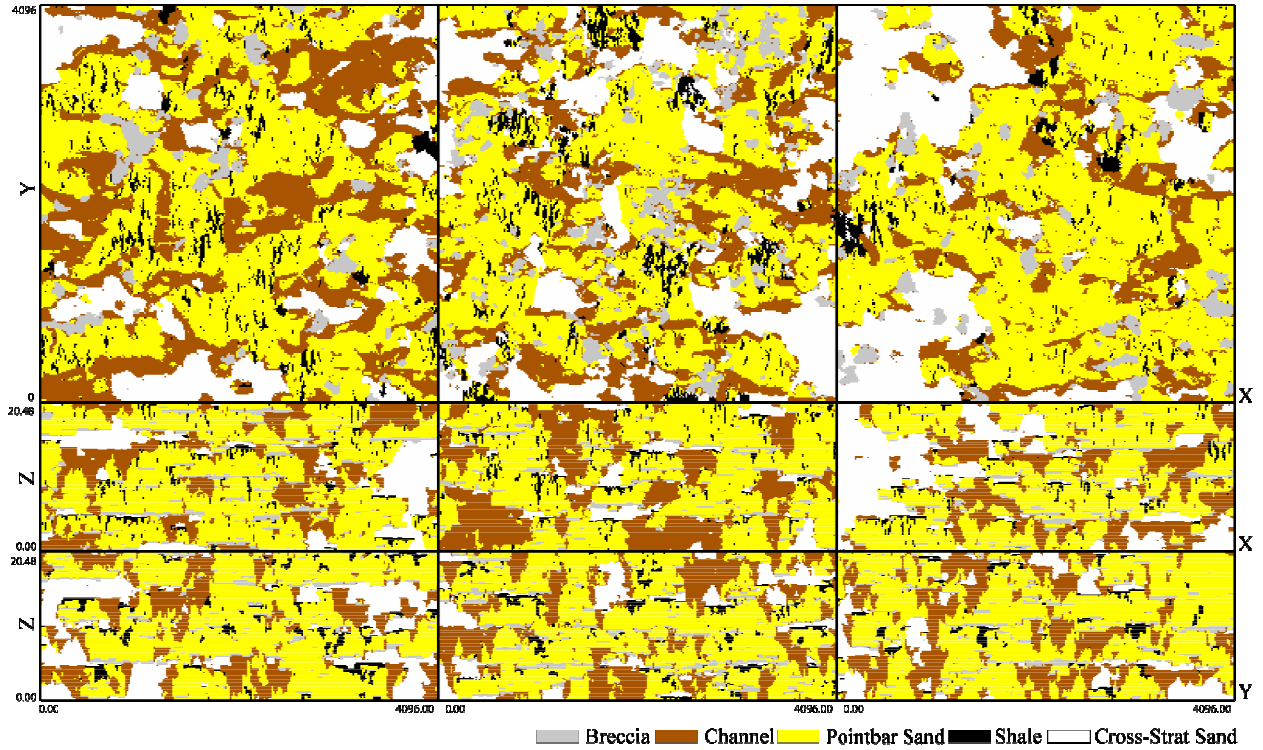


Figure 10: Estuarine SNESIM realization. From upper-left to lower-right: slice 24, 63, 100; XZ sections 43, 128, 213; YZ sections 43, 128, 243.

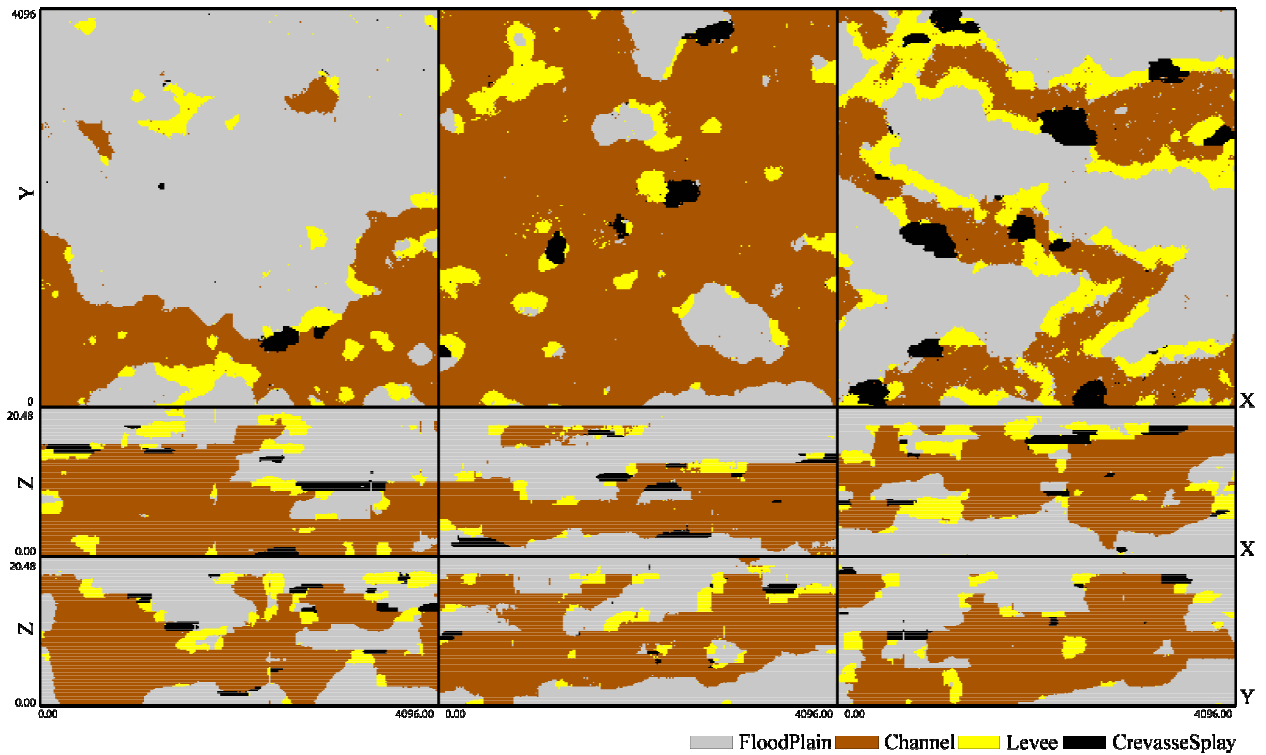


Figure 11: Fluvial MPS-GS realization. From upper-left to lower-right: slice 4, 44, 112; XZ sections 43, 128, 213; YZ sections 43, 128, 243.

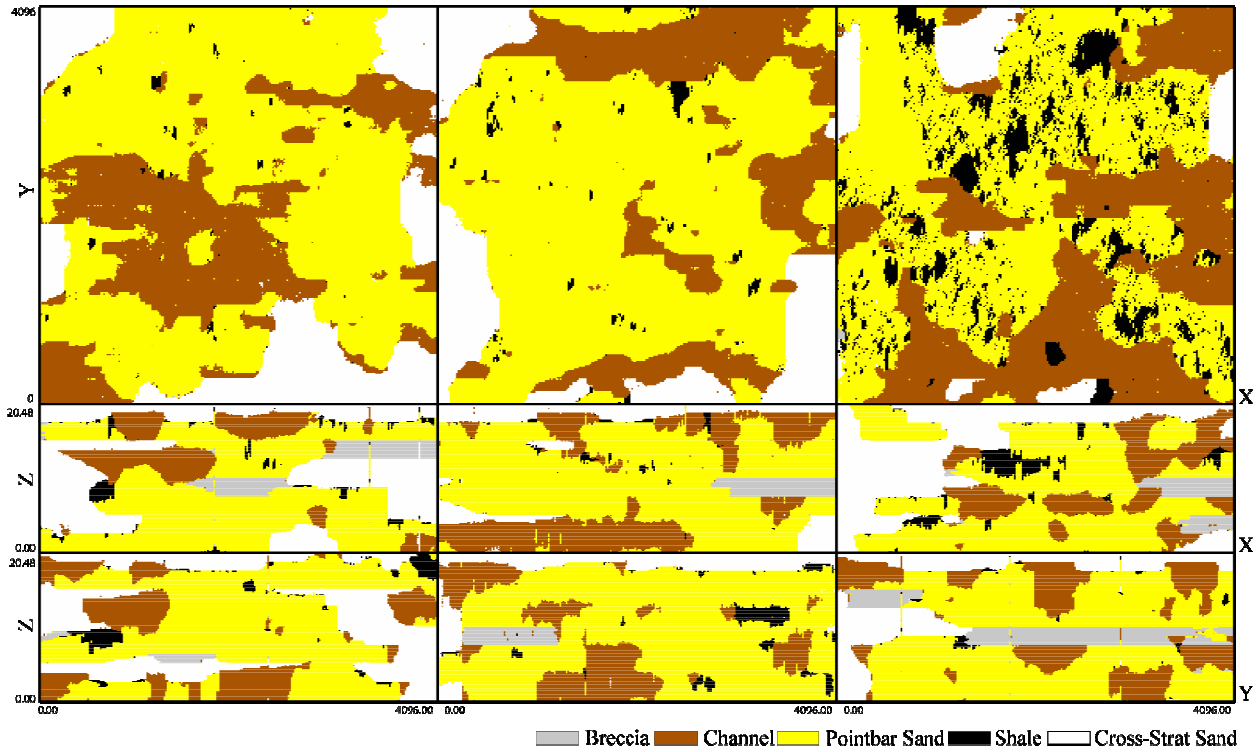


Figure 12: Estuarine MPS-GS realization. From upper-left to lower-right: slice 24, 63, 100; XZ sections 43, 128, 213; YZ sections 43, 128, 243.